

PAPER • OPEN ACCESS

CL as a tool for device characterisation: the case of laser diode degradation

To cite this article: S Dadgostar *et al* 2021 *Nano Ex.* 2 014001

View the [article online](#) for updates and enhancements.

You may also like

- [Mechanical and tribological performance of Al-Fe-SiC-Zr hybrid composites produced through powder metallurgy process](#)
G R Raghav, Sheeja Janardhanan, E Sajith et al.
- [Preparation of high molecular weight thermoplastic bio-based phenolic resin and fiber based on lignin liquefaction](#)
Yu Ren, Xu Lin, Wenlin Wang et al.
- [Comparative study between pure and manganese doped copper sulphide \(CuS\) nanoparticles](#)
Jiten P Tailor, S H Chaki and M P Deshpande



PAPER

CL as a tool for device characterisation: the case of laser diode degradation

OPEN ACCESS

RECEIVED

21 October 2020

REVISED

22 December 2020

ACCEPTED FOR PUBLICATION

15 January 2021

PUBLISHED

22 January 2021

S Dadgostar , J Souto and J Jiménez

GdS Optronlab, Ed. LUCIA, Paseo de Belén 19, Universidad de Valladolid, 47011 Valladolid, Spain

E-mail: jimenez@fmc.uva.es**Keywords:** laser diodes, catastrophic optical degradation (COD), dark line defects (DLDs), hyperspectral CL

Original content from this work may be used under the terms of the [Creative Commons Attribution 4.0 licence](#).

Any further distribution of this work must maintain attribution to the author(s) and the title of the work, journal citation and DOI.

**Abstract**

Cathodoluminescence is a powerful technique for the characterization of semiconductors. Due to its high spatial resolution, it is emerging as a suitable method for the study of semiconductor devices. The reduced dimension of the devices and the multilayer structure of their active parts demand experimental means with high lateral resolution and probe depth tunability for characterising the different layers forming the device structure. Degradation is a crucial technological issue for high power devices. In particular, the failures of laser diodes are due to the formation of defects during the laser operation. Those defects can be imaged by cathodoluminescence; furthermore, its spectroscopic capabilities permit to go beyond the mere observation of the non-luminescent area morphology, allowing a better understanding of the physical mechanisms of degradation. We present herein an overview of the cathodoluminescence analysis of catastrophically degraded high power laser diodes, both single mode and multimode broad emitter lasers. The study of the defects responsible of the degradation is a step forward to establish models of degradation, necessary to improve the laser power and durability.

1. Introduction

Luminescence techniques are currently used for the characterization of semiconductors. Photoluminescence (PL) was, and still is, a fundamental tool for the study of semiconducting materials [1–3]. As the device size decreased, the interest to get local information about the semiconductor properties was increasing, and the spectroscopic attributes of the PL were combined with the local character provided by the optical microscopes, which resulted in the development of micro PL, and PL mapping techniques [4–8]. The excitation with optical probes is achieved via a focused laser beam; therefore, the spatial resolution is limited by optical diffraction. According to the Rayleigh criterium the spatial resolution lies in the order of the light wavelength. This resolution is clearly insufficient for the actual sizes of the devices, as the local inhomogeneities of the semiconductor materials are relevant for the device operation and reliability. Therefore, there is an increasing demand for improving the spatial resolution of the luminescence probes in order to study the local fluctuations of certain properties, e.g. composition, and impurity distribution, but also the presence of non-radiative recombination centers (NRRCs), which are critical to the performance and failure of the devices [9, 10]. In this context, one needs to scale down the spatial resolution of the luminescence emission, as it remains a powerful technique of characterization, in order to study local aspects. When using a focused laser beam as the excitation source, one averages the luminescence response over a microscopic volume of the sample. Furthermore, most of the devices are formed by a multilayer structure, which consists of a stacked sequence of layers of different thicknesses and compositions; therefore, it is difficult to study these structures using optical beams, because the light penetration depth is limited by the absorption coefficients, and often the deepest layers are not accessible to the light beam. Most of these challenges can be addressed by cathodoluminescence (CL). With this technique, the excitation of the luminescence is performed by means of an electron beam [1, 11–15]. On one side the electron beam size lies in the range of a few nanometers and, on the other the penetration depth can reach up to

2–3 μm depending on the energy of the probing electrons, instead of the few hundreds of nanometers (≈ 100 – 200 nm) typically probed by the optical beam in PL measurements. Therefore, by changing the excitation approach, electrons versus photons, one improves the spatial resolution, even though the carrier diffusion also contributes to the spatial resolution. By varying the e-beam energy one can selectively study the different layers typically forming a device structure. A review about the study of heterostructured layers using CL can be found in [16].

Reliability is a very important issue in terms of safety and cost of electronic and optoelectronic devices, and, particularly, for high power devices [17, 18]. Most of the failures in these devices are associated with defects in the epitaxial structure, and those generated during operation, which lead to unattended failure, are particularly harmful because they are very difficult to screen. The degradation usually takes place at weak points of a device and are localized at a microscopic or submicroscopic scale [19–21]; therefore, the use of an experimental technique with high spatial resolution to study these defects is of crucial interest for improving its reliability. For example, dislocations are responsible for the early breakdown of GaN/Si-based power electronic devices [22]. Another example of the capacity of the CL technique for device failure analysis was reported in [23] for the study of high frequency, high power AlGaIn/GaN high electron mobility transistors (HEMTs).

Temperature device operation is a key parameter to understand the degradation. Generally, the degradation starts in a tiny hot spot. Therefore, measurement of the local temperature is of great relevance. It has been evaluated by micro-Raman spectroscopy, with a spatial resolution limited by the laser beam diameter (slightly submicrometric) [24]. The measured experimental temperature represents an average over the probed volume, so that local temperature might be significantly higher depending on the thermal conductivity around the hot region, which is specially critical in multilayer structures where thermal boundary resistances at the interfaces can lead to sharp temperature gradients [25]. Also, temperature data can be derived from the shift of the near band edge luminescence emission (NBE), e.g. using the shift of the intrinsic CL emission in GaN [26]. It should be noted that the excitation e-beam current is negligible with respect to the device operation current; therefore, no distortion is introduced by the electron beam during the CL measurements on devices under operation.

Device failure is related to the formation of defects behaving as NRRCs. Non-radiative recombination (NRR) produces heat, which is transferred to the lattice, or creates new defects by the mechanism of recombination enhanced defect reaction (REDR) [27]. The study of these defects is essential to understand the failure causality. The degradation takes place at a very local scale, and mainly concerns the active parts of the device, which are exposed to thermal, mechanical, and electrical stresses during the device operation. In this context, CL appears as a very suitable technique for studying the defects generated during the degradation.

We present herein the application of CL to the analysis of catastrophically degraded high-power laser diodes. The catastrophic optical damage (COD) of edge-emitting laser diodes is the sudden drop of the optical power after many hours of regular operation [17, 18, 28–34]. This phenomenon is critical in high power lasers as the COD is driven by the self-absorption of the laser radiation, therefore increasing the risks of failure when increasing the power. Because of the practical impossibility of monitoring a laser to catch a random failure, the study of the defects generated by those failures appears as the main way to establish degradation scenarios. On the bases of these scenarios, models have to be built-up to delimit the clues of the degradation aiming to establish failure causality [35, 36]. Electron beam excitation techniques, CL and the electron beam induced current (EBIC) sister technique [37], are powerful tools for this purpose as they are sensitive to the presence of NRRCs. However, this is a ‘post-mortem’ analysis, that does not provide immediate conclusions about the physical mechanisms driving the process. One needs therefore going down from the defect analysis to the root causes leading to the laser failure. We focus herein on the study of the main defects produced by the COD in high power laser diodes using the CL technique, aiming to get an insight into the physics of failure. The use of these techniques for the study of laser diode failure dates from the early times of the laser diodes innovation. Both panchromatic CL (pan-CL) and EBIC images allowed the visualization of the non radiative recombination areas related to the defects that result from the laser degradation. Most of the CL studies about the degradation of laser diodes did not use the spectroscopic capabilities of the technique but focused on the observation of CL images revealing the defect patterns [38–46]. Spectrally resolved CL provides additional information in regard to the laser diode failure analysis; hence, the interest of doing spectrally resolved CL for studying degraded lasers will also be addressed.

2. Laser diodes

Laser diodes consist of multilayer structures, basically formed by an active zone with one or more quantum wells (QWs), and the waveguide formed by the two barrier layers surrounding the QW. Two cladding layers encompass the waveguide. There is also the n-doped substrate and the contact layer on top of the p-type cladding layer. The Fabry–Perot resonant cavity in edge-emitting lasers is formed by two mirrors at both ends of the laser.

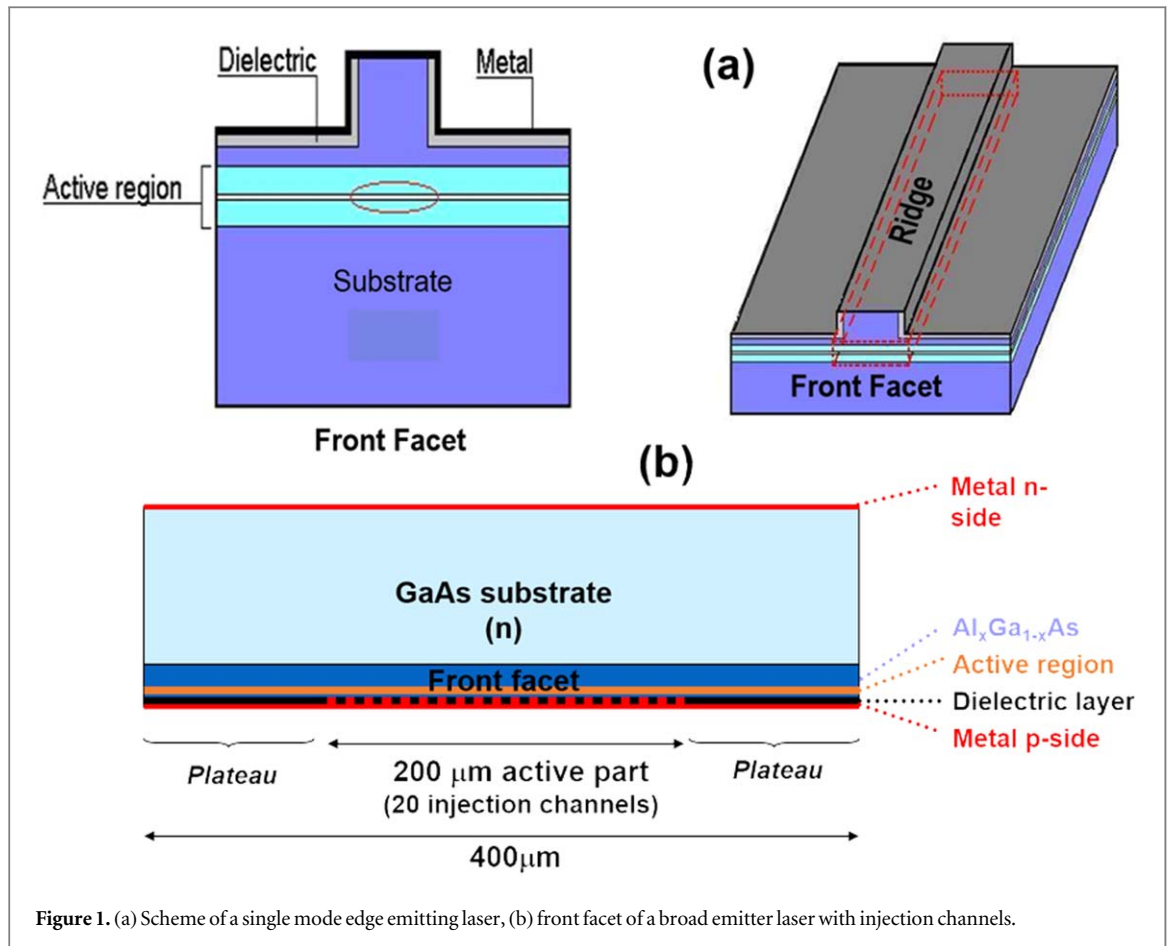


Figure 1. (a) Scheme of a single mode edge emitting laser, (b) front facet of a broad emitter laser with injection channels.

These mirrors consist of the cleaved (110) planes, which are coated with dielectrics in order to passivate the surfaces and provide the reflectivity necessary for optimizing the resonant cavity. The front facet is a low reflectivity (R) mirror, typically $R < 3\%$, while the rear mirror presents high reflectivity, typically $R > 95\%$. The mirror technology is critical in regard to the laser reliability as the mirror coatings do not only provide the required reflectivity but also protect the facets from oxidation. In order to reduce the QW optical load and the optical losses, the waveguide is generally asymmetric, the optical field being mainly guided by the n-type waveguide. The waveguide only supports one vertical optical mode, while the lateral optical modes are defined by a narrow ($\approx 3\text{--}5\ \mu\text{m}$) etched ridge for single-mode lasers, whereas broad emitters ($> 100\ \mu\text{m}$) are used in the case of multimode lasers, figure 1. There are different strategies to protect the mirrors, which, in general, are the weak parts of the laser. Usually, the region close to the mirrors is coated with a dielectric, up to a few μm s away from the mirrors, forming non injected regions (NIR). The lasers are soldered to a heatsink, either junction up or down. A typical high-power laser structure is formed by a QW surrounded by AlGaAs barriers and cladding layers, grown on an n-type GaAs substrate. Single-mode InGaAs/AlGaAs lasers can reach optical power densities as high as $80\ \text{MWcm}^{-2}$, while broad emitter lasers reach higher absolute power, typically a few tens of Ws, but lower power density and lower beam quality as compared to single mode lasers.

Laser degradation depends on the laser structure, operation conditions, laser beam energy, and the nature of the semiconductors constituting it [47]. Therefore, one can confront different degradation modes with a notable dispersion. We will focus here on high power lasers based on GaAs, in particular, high power 808 nm laser bars formed by 25 broad emitters with AlGaAs QW and graded index separate confinement heterostructures (GRINSCH) with output powers up to a few tens of watts. Besides, we will present the CL analysis of 980 nm single-mode strained InGaAs/AlGaAs QW pump lasers, which typically supply ≈ 1 watt of continuous-wave (cw) optical power. Each laser type presents different defect signatures after COD, even if some general trends do exist. Both of these types of lasers have high technological relevance. In particular, the 808 nm laser bars are used for solid-state laser pumping, metal and plastic welding, hard and soft soldering, and surface treatments among other applications. These applications do not need high beam quality; that makes laser bars a good option for providing high optical power. Regarding the single-mode 980 nm lasers, they are the basic devices for pumping Er-doped fiber amplifiers, for which a high-quality beam (monomode) is necessary.

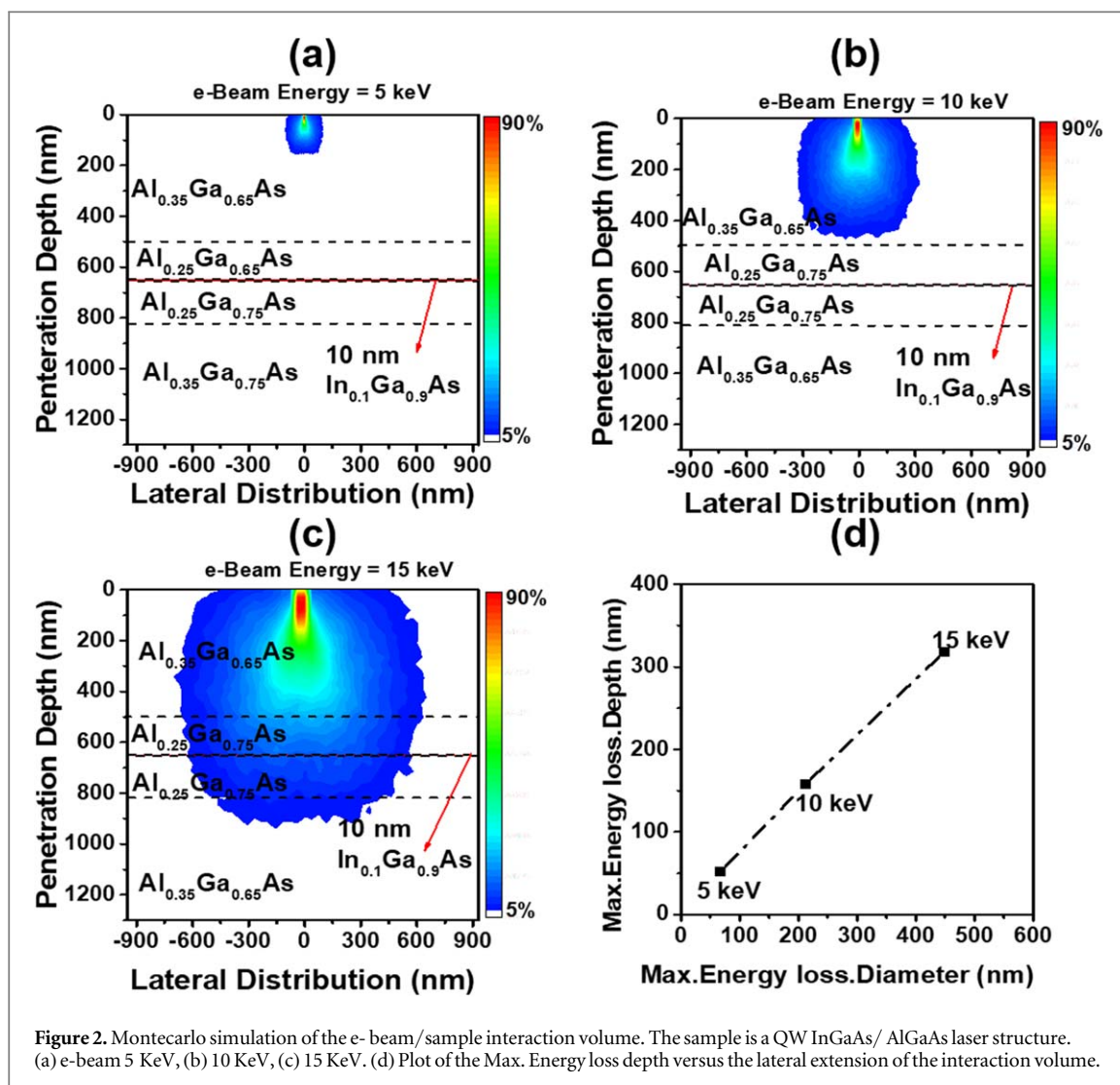


Figure 2. Monte Carlo simulation of the e-beam/sample interaction volume. The sample is a QW InGaAs/ AlGaAs laser structure. (a) e-beam 5 KeV, (b) 10 KeV, (c) 15 KeV. (d) Plot of the Max. Energy loss depth versus the lateral extension of the interaction volume.

3. Spatial resolution

One of the critical issues of the CL applied to the laser degradation study is related to the spatial resolution, which is crucial as far as the laser failure appears as a local event. The spatial resolution of the CL technique is a complex problem to which abundant literature is devoted [11–15, 48].

When optimal conditions are fulfilled, resolutions of a few tens of nanometers can be achieved. The spatial resolution of CL is governed by several experimental parameters, as well as the nature of the samples. Among the experimental parameters, one can distinguish the size of the e-beam, the energy of the electrons, and the working distance. In fact, the e-beam size of field emission scanning electron microscopes (FESEMs) can be reduced to a few nm in diameter. However, this does not define the spatial resolution, as one has to refer to the electron-hole pair generation volume, which is determined by the spatial extension of the e-beam/sample interaction [49, 50].

Regarding the working distance, one has to consider that it is increased with respect to the conventional microscope mode (secondary electrons image) because one needs to intercalate the collection optics between the microscope lens and the sample, which is not necessary for EBIC measurements that are collected in similar conditions as secondary electron (SE) images. The beam size is much smaller than the beam/sample interaction volume. In fact, when the primary electrons enter the sample, they lose their energy in successive collisions, with the result of the spreading of the e-beam inside the sample. The trajectory of electrons inside the sample can be calculated using Monte Carlo simulations [51]. The interaction volume depends on the parameters of the e-beam and the characteristics of the sample. The higher the e-beam energy, the deeper the penetration of the electrons. As the beam penetrates it spreads laterally. The larger the e-beam energy the larger the lateral spreading, thus reducing the lateral resolution. Therefore, the highest spatial resolution is achieved with low energy e-beams. Hence, in multilayer structures, such as the laser diodes, the highest spatial resolution can only be reached on the closest layers to the surface, while the deepest layers need higher e-beam energies to excite their luminescence. In particular, the study of the QW and the n-type barriers and claddings in plan view must be done with a

sufficiently high e-beam energy. Therefore, the exploration of the QW, critical to the study of the laser degradation, implies a certain loss of lateral resolution with respect to the resolution that one can reach on the layers closest to the surface, i.e., the top p-cladding and the contact layers.

The interaction volume for different e-beam energies is calculated for an InGaAs/AlGaAs QW laser structure using CASINO software [51], figures 2(a)–(c). One can see the close relationship between penetration depth and the lateral extension of the generation volume. One can also observe the need for increasing the e-beam energy to reach the QW. The penetration depth (taken as a third of the electron range, $R/3$) plotted versus the lateral size of the interaction volume is shown in figure 2(d), evidencing the compromise between probe depth and lateral resolution.

Another factor that can affect the spatial resolution concerns the distribution of the generated e-h pairs. The role of carrier diffusion in the spatial resolution of CL has been largely discussed [52–55]. In principle, because of the large numerical aperture mirrors used for collecting the CL, one can assume that there is a divergence between the e-h generation volume and the luminescence emission volume because the light emitted by the recombination of the carriers out-diffusing away from the generation volume can be collected by the mirror. Donolato demonstrated that the carrier diffusion does not substantially enlarge the carrier distribution volume, as the carrier density decreases faster than the exponential law usually reported for the carrier diffusion [56]. On the other hand, when recording CL images, one aims to reveal the presence of defects, which often behave as NRRCs, e.g. dislocations. The carrier diffusion length around these defects is drastically reduced, and, therefore, the steady state carrier distribution in their vicinity is not substantially enlarged by diffusion. In fact, the recombination atmosphere of individual dislocations can be revealed by CL images with a high spatial resolution [57–59]. The ability of CL to resolve tiny inhomogeneities is tightly related to the steady state distribution of the generated carriers inside the generation volume. Defect features smaller than the diffusion length have been experimentally imaged by CL. Paraphrasing P.R. Edwards et al: ‘what the CL is imaging is at least partially the variation in carrier diffusion itself’ [60]. This variation is related to the presence of features locally reducing the diffusion length, e.g. recombination at dislocations, or the potential barriers at the interfaces. Thus, one can image by CL the recombination atmosphere of individual dislocations, or a few nm thick QWs, or nanorods [57–59, 61, 62]. As an example, CL images of both isolated and clustered dislocations in InGaN are shown in [58]. The resolution of individual dislocations requires a separation between them at least larger than the diameter of the e-h generation volume.

4. Laser failure

The failure of laser diodes can be classified into three different degradation modes: gradual, rapid, and catastrophic [17, 18, 63–65]. Both the type of defects and the degradation sequence differ from each other. The gradual mode is the typical wear out process dealing with the formation of point defects, small precipitates, and dislocation loops, which slowly, and progressively degrade the laser parameters over long periods of operation. Rapid degradation can be easily screened by burn-in tests [47]; it appears as a sharp drop of the laser optical power in a time scale of hours, usually associated with the presence of dislocations in the active zone of the laser. These dislocations propagate during laser operation forming large areas of reduced luminescence emission. Meanwhile, the catastrophic degradation corresponds to a sudden loss of optical power, in a scale of seconds or less. This mode is usually identified as the catastrophic optical damage (COD). The COD appears shortly after reaching a critical temperature at the front facet or inside the cavity [31, 66]. We will focus herein on the CL analysis of lasers that suffered COD, in order to reveal the defects issued from the degradation, as a means to understand the mechanisms driving this process.

The COD is usually associated with a thermal runaway process [39]. It can occur either at the mirror facet or inside the laser cavity [67], labeled as catastrophic optical bulk damage (COBD), in contraposition to the more frequent facet mirror damage usually labeled COMD. COBD occurs in lasers for which the improved facet technology enhances the resilience to COD of the mirror facets. The thermal runaway is usually described in the literature as follows: on a first stage the temperature is locally enhanced, with the corresponding local bandgap shrinkage; therefore, the transparency regime is lost at that hot spot. Then, laser self-absorption further increases the temperature with the concomitant absorption, leading to melting in a positive feedback loop [39, 68]. This picture neglects some aspects of the mechanisms leading to the fast degradation occurring under COD. In particular, the relation of COD with the gradual aging, the origin of the local heating, which is the ultimate cause launching the COD, the meaning of the critical temperature, and the mechanisms leading to the thermal runaway and its relation with the thermal, optical and mechanical properties of the active zone of the laser [25, 66, 69–71]. Because of the virtual impossibility to monitor the sequence of COD in real-time, the study of the defects formed under the COD process is the main way to set up a physical model for the degradation.

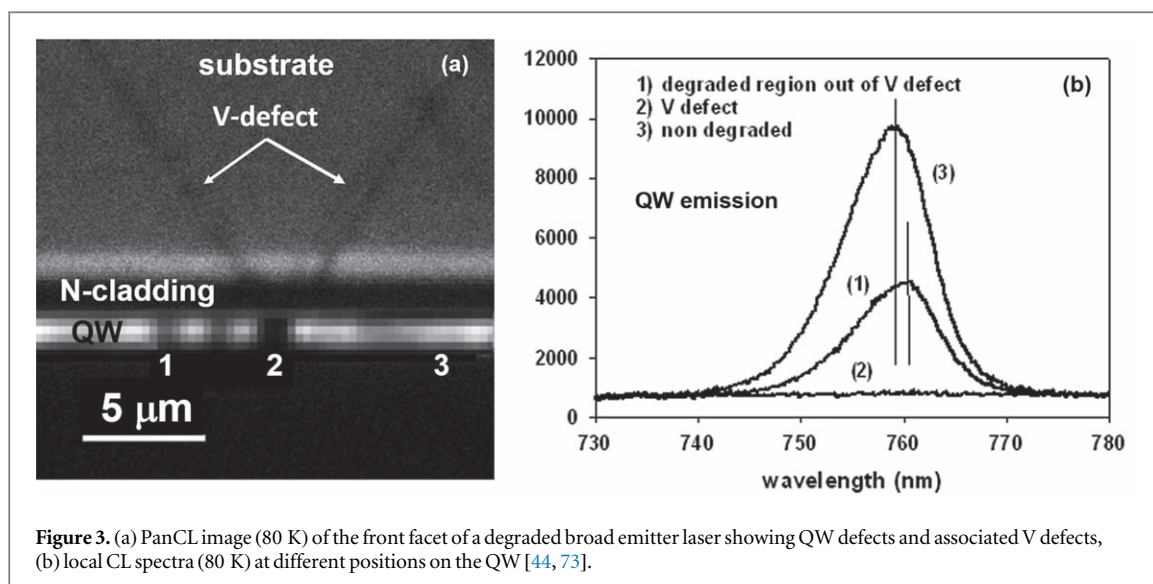


Figure 3. (a) PanCL image (80 K) of the front facet of a degraded broad emitter laser showing QW defects and associated V defects, (b) local CL spectra (80 K) at different positions on the QW [44, 73].

5. Cathodoluminescence of degraded laser diodes

The study of the degradation requires the investigation of the main defects generated during the laser operation. The identification of the defect signatures in degraded devices is crucial to establish the physics behind the COD process.

As we have already mentioned, COD is a random failure extremely difficult to analyze in real-time, as it can occur unexpectedly after thousands of hours of regular operation. Therefore, one needs to proceed by accelerated aging tests. COD can be accelerated by increasing the current and the optical power. Some devices fail once a threshold optical power is reached, the so-called power to COD [30]. In other cases, the optical power simply decreases as the temperature of the cavity increases for increasing current: this is the thermal rollover effect, which is a reversible process and does not concern laser degradation [65]. Accelerated tests can be performed at a high temperature in cw operation (burn-in test) which significantly reduces the time to failure [47]. Another aging approach is based on the use of stress step tests, which consist of the application of successive high current pulses of predetermined duration leading to COD [70, 72]. Also, one can use electrostatic discharge (ESD) tests, which is basically one single step test at a very high current.

EBIC has been more frequently used for the characterization of degraded lasers because it can be carried out without a specific preparation of the laser whenever the metal layer is thin enough to allow the e-beam penetration into the junction [41]. Unlike EBIC, CL needs of the preparation of the laser, as the contact metal layer has to be removed to allow the luminescence emission to emerge; also, the ridge is removed in order to have a flat surface giving a spatially homogeneous e-beam penetration.

6. Defect signatures of laser degradation

6.1. Multimode AlGaAs/GaAs lasers

The results of the COD can be visualized in pan-CL images as non-luminescent areas [38] associated with the defects generated during the laser degradation process, which behave as NRRCs. The pan-CL images give a similar contrast to the EBIC images as both are sensitive to carrier capture. However, CL may provide additional information when using its spectroscopic capabilities.

The devices referenced here are GRINSCH QW AlGaAs/GaAs laser bars emitting at 808 nm with output powers up to a few tens of watts. Typically, these bars consist of 25 emitters (200 μm wide) separated from each other by optically and electrically isolated channels, with a period between emitters of 400 μm . Each single emitter is divided into 20 injection channels separated by dielectric stripes with a period of 10 μm , figure 1. These bars are soldered p-side down, typically using a CuW heat sink with AuSn solder. The lasers described here have undergone burn-in aging test at a constant optical output power of 30 W. After the aging step, the lasers are separated into individual emitters. They are etched in a diluted HF solution, which removes the metal layer by under-etching the dielectric layer beneath the metal, thus opening the cavity to observation by CL. Both cross-section CL images of the front facet and plan-view CL images of the laser cavity are described here.

A panCL image of the mirror facet of a degraded emitter is shown in figure 3(a). The QW emission is imaged, and it shows a series of dark spots, corresponding to degraded zones. Note that the confinement of carriers in the

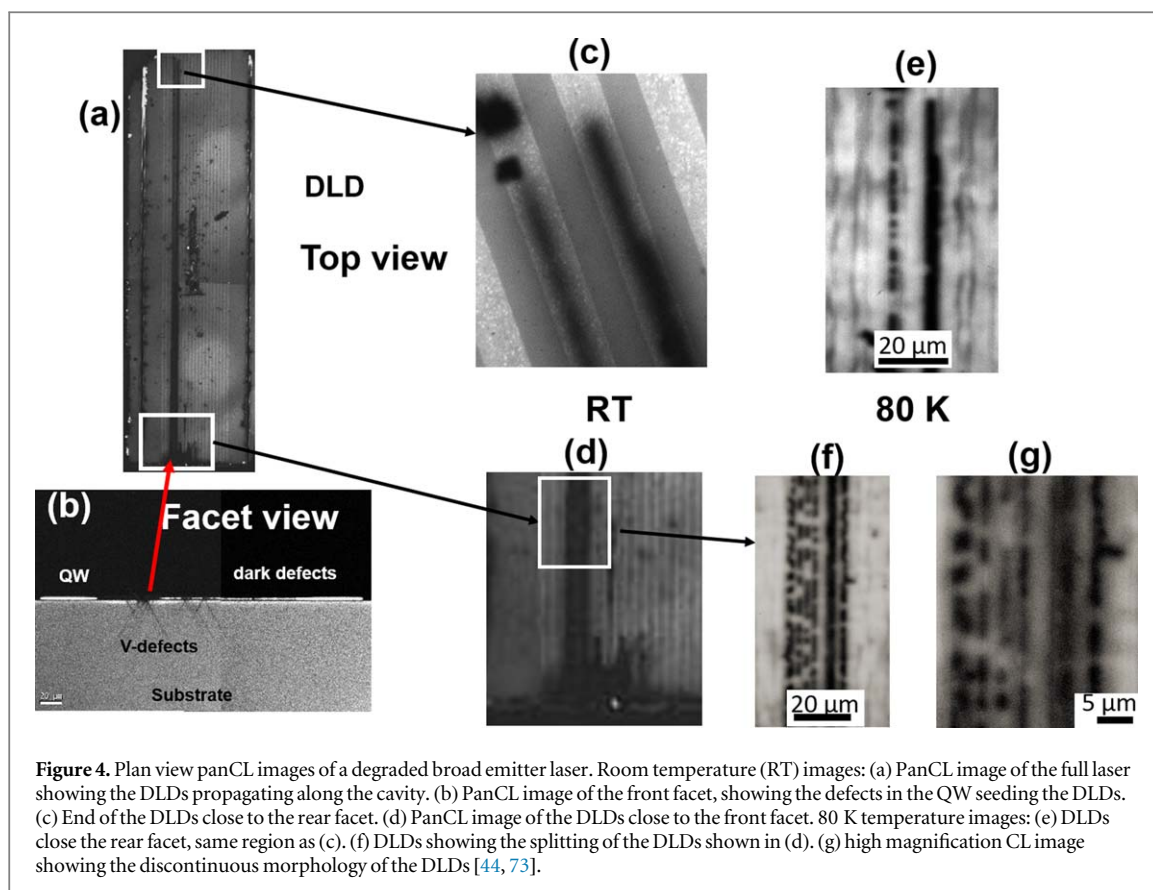
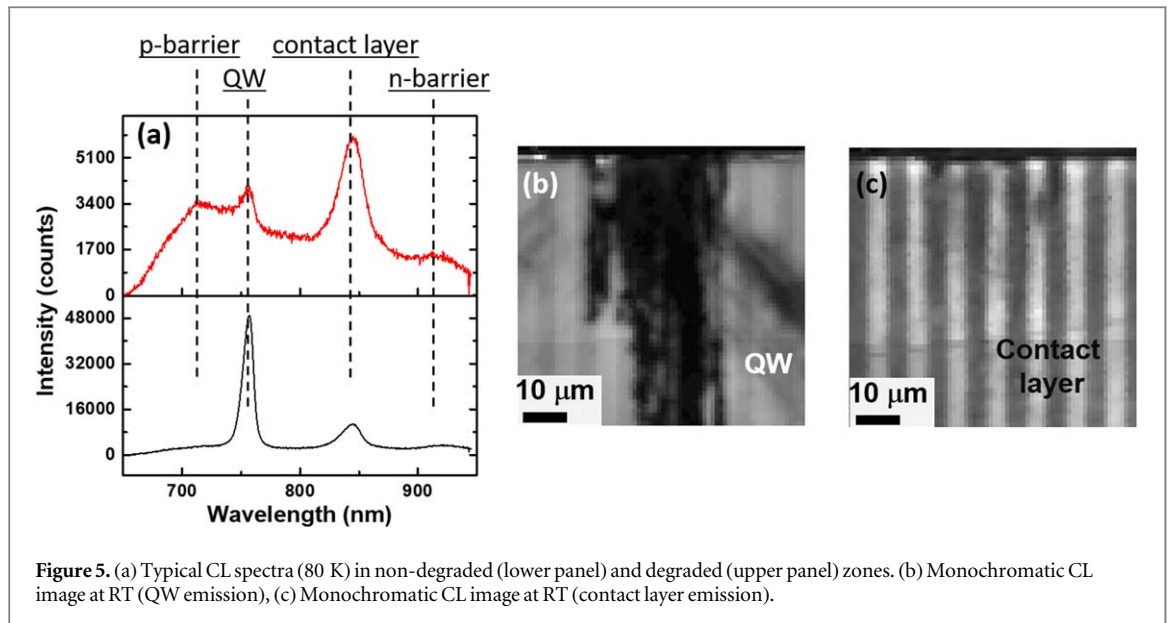


Figure 4. Plan view panCL images of a degraded broad emitter laser. Room temperature (RT) images: (a) PanCL image of the full laser showing the DLDs propagating along the cavity. (b) PanCL image of the front facet, showing the defects in the QW seeding the DLDs. (c) End of the DLDs close to the rear facet. (d) PanCL image of the DLDs close to the front facet. 80 K temperature images: (e) DLDs close to the rear facet, same region as (c). (f) DLDs showing the splitting of the DLDs shown in (d). (g) high magnification CL image showing the discontinuous morphology of the DLDs [44, 73].

QW permits to reach a spatial resolution equivalent to the QW thickness, so that the QW emission appears clearly differentiated in the CL image. Some of the dark spots are at the apex of V-shaped dark contrast structures propagating across the n-barrier and cladding layers, even reaching the substrate. These are the so-called V defects [73, 74]. The branches of the Vs form an angle of 57° with the epitaxial plane; therefore, they correspond to the intersection of the mirror plane (110) with the dislocation gliding plane (111). Parts of the QW are fully quenched, while others still luminesce exhibiting different degrees of quenching, which correspond to diverse levels of degradation. Local CL spectra at selected points of the QW in the front facet are shown in figure 3(b). The QW emission is fully quenched at the apex of the V defects, which accounts for the full destruction of the QW in these positions. On the other hand, QW dark contrasted zones without associated V defects are not fully quenched, which suggests that these regions are in an earlier stage of degradation with respect to the areas with associated V defects [73]. The V-shaped defects have been associated with the relaxation of the compressive stress induced by packaging [74, 75]. Maximum packaging stress is concentrated in the center of the soldered bar [47], with significant relaxation close to the bar ends. It is true that, statistically, the V-defects appear more often in emitters of the center of the bars, where the packaging stress is maximal; however, its presence is also observed in regions close to the ends of the bars where the packaging stress is almost fully relaxed. Besides, they are exclusively observed in aged lasers, which points to additional driving forces developed during laser operation being required for the V-defects to be generated. In particular, the local heating at the front facet during laser operation induces thermal stresses that, when associated with the packaging stress, might generate arrays of dislocations gliding along the (111) planes. Note that the V branches can penetrate deeply into the substrate, thus suggesting a strong stress field, and pointing to high-temperature gradients at the front facet. These large temperature gradients should be produced by local non-radiative recombination at certain zones of the QW in the front mirror, and subsequent laser radiation absorption. Symptoms of melting are often seen at the front facet, e.g. blisters of ejected material are observed in the optical microscope [76].

The non-luminescent areas seen inside the cavity in top view CL images adopt an elongated shape, the so-called dark line defects (DLDs) [39] running along the injection channels of the laser cavity, figure 4(a) [73]. DLDs start at the front facet at the same position where the apex of the V defect was formed. This suggests that the DLDs are seeded at the front facet in the most degraded points of the QW. The DLD propagation along the cavity is fueled by laser self-absorption; therefore, these DLDs follow the optical field instead of a particular crystal orientation.



While damage is initiated in the active zone of the laser, the QW, it might also extend to the waveguide and cladding layers. However, due to their composition, it cannot be seen in the panCL images because of the virtual lack of emission from the graded waveguides (26%–65% Al) and the cladding layers ($\text{Al}_{0.65}\text{Ga}_{0.35}\text{As}$). TEM images show the effective damage of the waveguide [77]. The DLDs propagate following the injection channels and can run along the cavity ending close to the rear mirror, figures 4(a), (c), (d). It is interesting to compare the CL images recorded at 300 K with those recorded at 80 K, figures 4(e)–(g). Surprisingly, the morphology of the DLDs, as viewed in the CL images, changes at 80 K. At room temperature one observes two continuous, slightly blurred, DLDs propagating along two contiguous injection channels; however, at 80 K one observes that the DLDs split in several parallel well resolved dashed lines forming discontinuous sequences of aligned dark contrasted short segments separated from each other by $\approx 3\text{--}4\ \mu\text{m}$ of less damaged material. These parallel dashed lines can be associated with the filamentation of the optical modes by the effect of local heating [78]. This difference between the CL images at 80 K and 300 K is probably the consequence of the higher carrier diffusion length at room temperature, which blurs the discontinuous defect line observed at 80 K into a continuous line at room temperature. Also, this observation calls into question the mechanisms of propagation of the DLDs. The discontinuous nature of the DLD rules out the hypothesis that a DLD is generated by the propagation of a molten front, as it has been formerly claimed [39]. The propagation of a molten front was indeed observed in InGaAsP/InP laser structures [40]. The epilayer structure was pumped with a heavily absorbed Nd:YAG laser (1064 nm), at a very high optical power density, $100\ \text{MW cm}^{-2}$, much higher than the laser diode optical power density. The DLD was nucleated at crystal defects. This rules out any similarity with the DLDs generated under laser operation. The propagation of the DLDs seems to obey more complex mechanisms than mere melting. On the other hand, this discontinuous degradation pattern shows similarities with the degradation of InGaAs/AlGaAs lasers, as we will see later.

Complementary information can be unveiled by using the spectroscopic capabilities of CL. Typical CL spectra recorded at different points of a hyperspectral CL image are shown in figure 5(a). One observes the QW emission at $\approx 760\ \text{nm}$ (note that the spectrum was recorded at 80 K, which accounts for the blue shift with respect to the nominal laser emission), the contact layer emission at $\approx 845\ \text{nm}$, a weak feature at $\approx 720\ \text{nm}$, which should be associated with the barrier layer emission, and a broadband at $\approx 920\ \text{nm}$. Processed hyperspectral images reveal that the contact layer is not damaged, figures 5(b), (c). The distributions of the QW emission and the 920 nm band are spatially correlated: the 920 nm band is quenched when the QW emission is quenched. PL emission at $\approx 918\ \text{nm}$ (1.35 eV) related to $V_{\text{Ga}}\text{-Si}_{\text{Ga}}$ pair complexes has been reported for both metal-organic chemical vapor deposition (MOCVD) [79, 80] and molecular beam epitaxy (MBE) [80, 81] Si-doped $\text{Al}_x\text{Ga}_{1-x}\text{As}$ ($x = 0.3$); therefore, this emission can be related to the n-type barrier layer, as it is Si-doped. The spatial correlation with the QW emission might suggest that the damage generated in the QW extends to the n-type AlGaAs barrier layer. The 720 nm emission is probably related to the p-type barrier layer. The 720 nm CL emission is anticorrelated to the QW damage pattern, it presents bright contrast in the dark contrasted zones of the QW emission image. The enhanced emission from the p-barrier layer suggests that the damage is not severe in the p-barrier; therefore, one can claim that the damage associated with the COD process in these lasers mainly concerns the QW and the n-type waveguide layer. It should be noted that the bar is soldered p-side down, which should allow a better heat dissipation in the p-side.

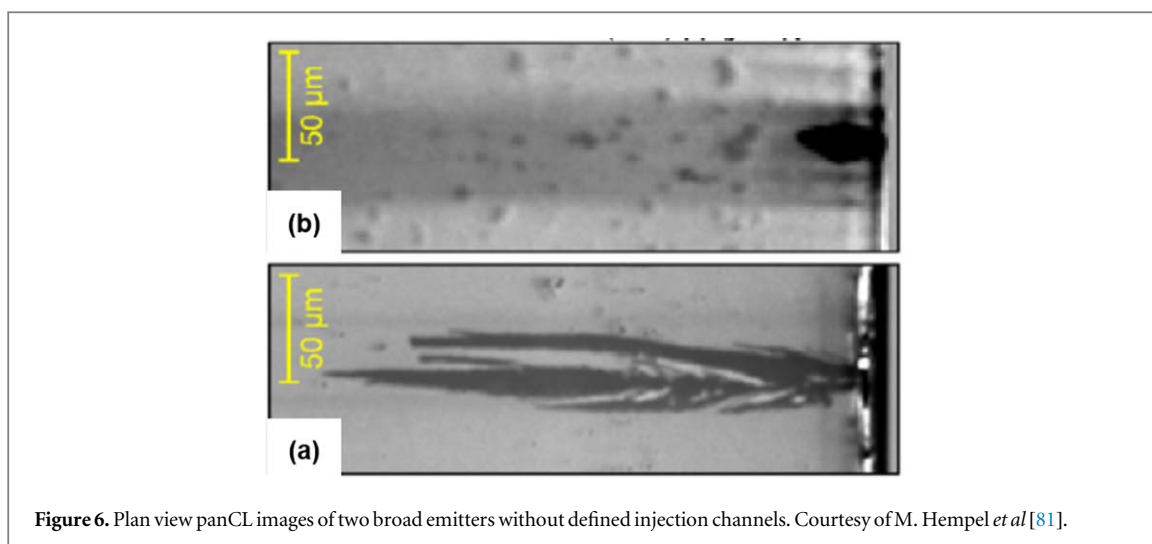


Figure 6. Plan view panCL images of two broad emitters without defined injection channels. Courtesy of M. Hempel *et al* [81].

In the absence of injection channels, the DLD pattern of a broad emitter presents a different shape. Figure 6 shows the CL image of a catastrophically degraded 808 nm broad emitter laser, where one can appreciate that the DLDs do not follow the same path as in figure 4 [81]. This is due to the different distribution of the laser modes in the two laser configurations. In the laser of figure 4 the optical modes are guided along the injection channels, while in the broad emitter without the injection channels the optical modes can be deviated and superposed during the degradation, locally increasing the effective optical power and resulting in defect propagation patterns as those shown in figure 6. A study of the degradation of broad emitter lasers using EBIC, and a model describing the formation of this defect pattern was reported elsewhere [82].

6.2. Single-mode lasers, strained InGaAs QW lasers

Strained QW InGaAs/AlGaAs lasers present several advantages, e.g. low current threshold, high power density, and improved reliability, that render them the most efficient and reliable high-power laser diodes available. For a time it was claimed that they were immune to COD [83]. However, as the optical power of these devices increased, COD started to be observed as well in this type of lasers. Usually, the waveguide structure is asymmetric. This is achieved by controlling the refractive indexes of the two barrier layers, n and p, so that a higher optical power fraction is carried by the n-type waveguide, roughly 60% versus 30% (p-type). The QW also carries a lower optical power density than the n-type guide. This distribution of the vertical mode permits a significant reduction of the optical losses, and, in particular, a lower absorption by the QW, which is the potential absorbing medium during laser operation, and therefore the layer where degradation would start.

High power single ridge waveguide InGaAs/AlGaAs QW lasers (GRINSCH 980 nm lasers) are formed by a strained InGaAs QW ($\approx 10\%$ – 15% In), AlGaAs barriers with Al fraction ranging from ≈ 0.1 to 0.3 , and cladding layers with $x \approx 0.3$. The lateral mode is limited by a narrow ridge (3 – $5 \mu\text{m}$ wide), figure 1. Under cw operation the COD power threshold slowly decreases as a consequence of the generation of point defects during the laser aging. However, this can take a long time, up to thousands hours, and therefore, accelerated tests are used to provoke the COD. In particular, COD can be induced by different aging procedures, e.g. repetition of short single current pulses of increasing current [70]. It is admitted that this procedure creates a defect pattern similar to the one observed in long term COD. Therefore, accelerated aging tests have been used to study the defect formation during COD. These accelerated tests act on fresh devices, while the long-term COD takes place on devices with a non-residual presence of point defects generated during many hours of operation. Even if the defect signature is similar, one might say that the dynamics leading to the COD must be different depending on the aging scenarios; however, one can learn about the physical mechanisms of COD using accelerated aged devices. In particular, we consider lasers aged during burn-in tests, and lasers that have suffered a voltage transient leading to COD.

As previously mentioned, once the metal layer has been removed, the ridge is eliminated rendering the top surface planar. First, one must observe the degraded devices at the SEM to detect morphologic changes that could be produced during the preparation process. Only one of the lasers subjected to electrostatic discharge (ESD) suffered morphologic changes, revealed by the etching procedure to prepare the planar surface. None of the other lasers showed external morphology changes. All the lasers present DLDs aligned along the ridge in the CL images.

The ESD aged laser presents evidence of melting close to the rear facet. It is well known that electrical transients applied in ESD tests can introduce changes in the junction of devices due to localized heating associated with local current crowding [83, 84]. Starting from the molten zone a DLD propagates towards the front facet. On the other hand, the DLDs observed in lasers aged by burn-in tests are initiated close to the front

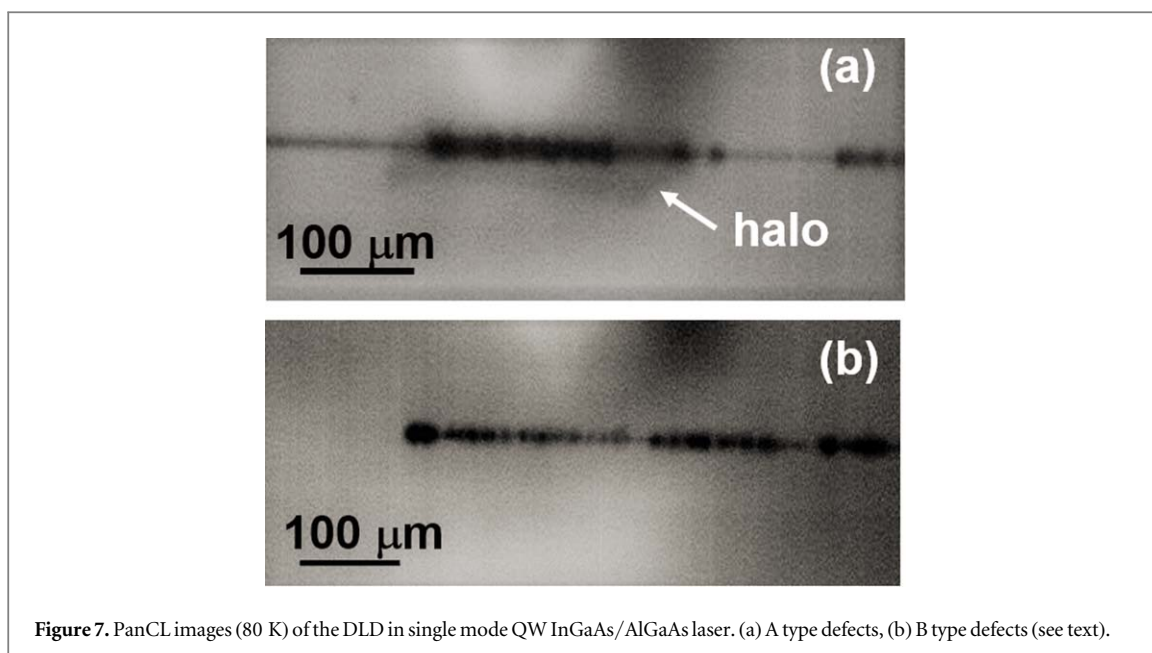


Figure 7. PanCL images (80 K) of the DLD in single mode QW InGaAs/AlGaAs laser. (a) A type defects, (b) B type defects (see text).

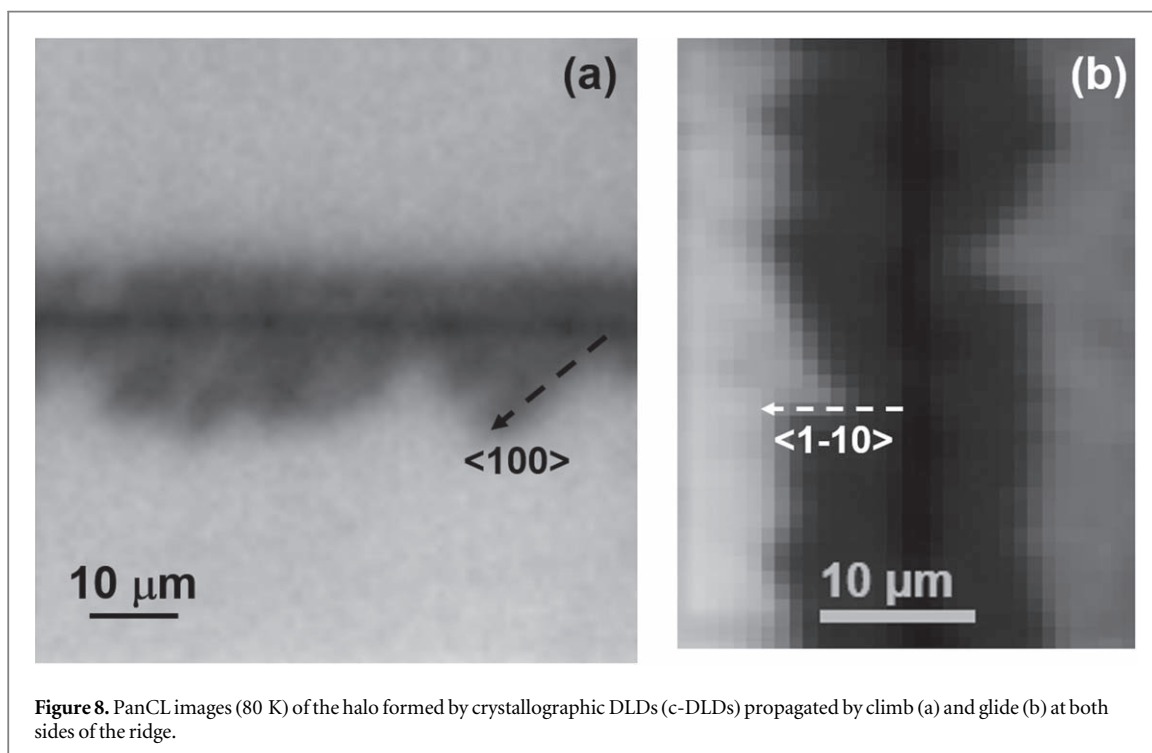


Figure 8. PanCL images (80 K) of the halo formed by crystallographic DLDs (c-DLDs) propagated by climb (a) and glide (b) at both sides of the ridge.

facet and extend over a distance close to the half-length of the cavity. Finally, lasers aged by voltage transients present a dark line placed around the middle of the cavity, shorter than the ones observed in the lasers suffering burn-in aging.

The DLDs as observed in the pan-CL images are not uniform, but they present different shapes along the cavity, revealing different defect distributions which account for different mechanisms of interaction between the optical field and the active layers of the laser. A quasi-continuous DLD can be observed. In certain zones, the DLD appears continuously forming a true dark line, while other parts of the DLD are formed by a series of aligned dark spots. In fact, the non-uniformity of the DLDs along the laser cavity seems to show different levels of degradation. One can distinguish two different defect patterns along the DLD, figure 7. We label them as A type and B type, respectively.

When looking in detail to the A type defects of, one observes that the dark line running along the ridge is surrounded by a halo spreading at both sides of the ridge, figure 7(a). The halo consists of a cloud of dislocations, forming DLDs oriented along crystallographic directions, either perpendicular to the laser cavity, $\langle 1-10 \rangle$ oriented, or aligned along the $\langle 100 \rangle$ crystal axis forming 45° with the cavity axis, figure 8. These networks of

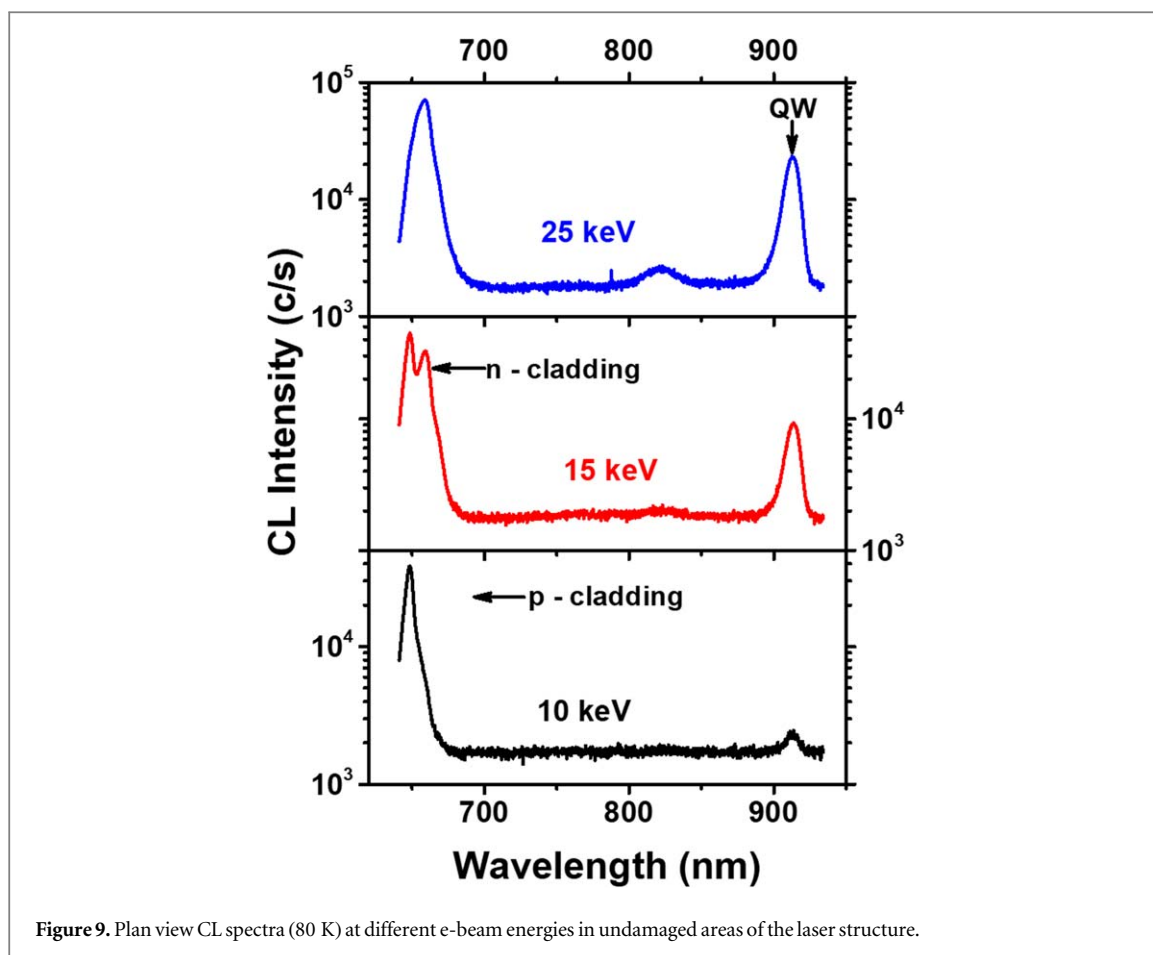


Figure 9. Plan view CL spectra (80 K) at different e-beam energies in undamaged areas of the laser structure.

dislocations propagate during the laser operation by either glide ($\langle 1-10 \rangle$) or climb ($\langle 100 \rangle$) [85–88]. We label these DLDs as crystallographic (c-DLDs) because, opposite to the main DLD oriented along the laser cavity, they follow crystallographic directions, and propagate according to the classical mechanisms of climb and glide, described in previous studies about the degradation of double heterostructure (DH) lasers [85–88].

When dealing with B type defects, the DLD presents a discontinuous dotted shape, with a slight lateral broadening of the darkest dots, which are separated by zones with a lower dark contrast, figure 7(b). The lateral spreading of the dark contrast areas in the darkest dots is different from the halo observed in A type defects. The QW emission is partially quenched in this DLD morphology, with the CL intensity profile along the ridge showing a very irregular pattern of QW emission, unlike the A type defects, which show a pronounced quenching of the QW emission along the ridge.

The morphology of the DLDs aligned along the laser cavity as revealed by the CL images suggests different stages of degradation depending on the zones of the DLD resulting from the interaction between the optical field and the laser cavity. When the QW CL emission appears fully quenched, one can assume that it contains a high concentration of defects, e.g. dislocations. In fact, under the thermal stresses induced by the local heating, the active zone should collapse into a dense array of dislocations, which give the dark contrast of the CL images. It has been claimed that these quenched zones are the result of melting and subsequent recrystallization [39], and that the DLDs are formed by the propagation of the melting front. However, the discontinuous nature of the DLDs with different levels of degradation along them does not support such a statement. Local melting can occur but as an ultimate consequence of the interaction between the laser beam and the dense tangle of dislocations formed prior to melting [69]. In this sense, this presents similarities with the degradation of the 808 nm lasers previously described.

The defects revealed by the CL images constitute the fingerprint of the degradation. One needs to unravel where the defects are localized, and how is the luminescence emission of the different zones of the DLDs, as they present different signatures. First, one needs to interpret the CL spectrum of the laser structure. By varying the e-beam energy one can selectively excite the different layers forming it, thus allowing the identification of the origin of the luminescence bands. CL spectra of a pristine laser structure recorded with different e-beam energies are shown in figure 9. The spectrum excited with 10 keV electrons shows a CL band peaking at 649 nm, and a very weak band peaking at 916 nm. These bands correspond respectively to the top p-type cladding layer (649 nm), and the QW (916 nm instead of the 980 nm nominal laser light, because the spectra are recorded at

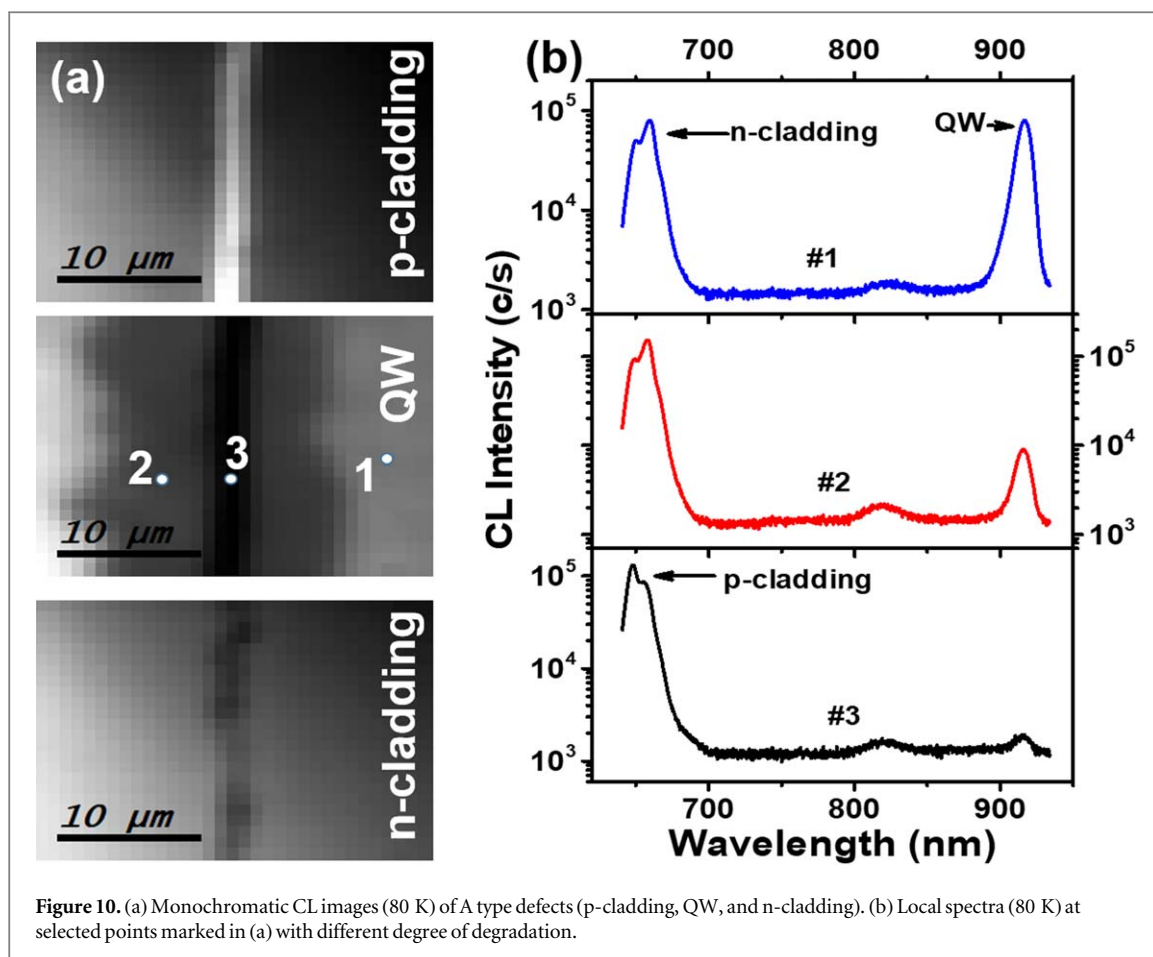
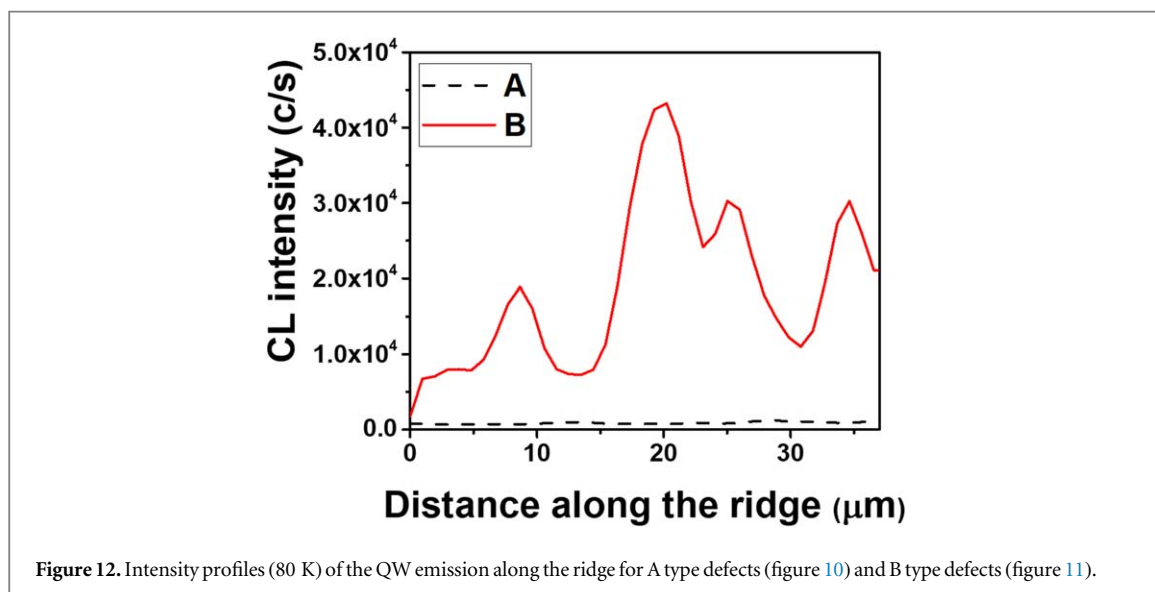
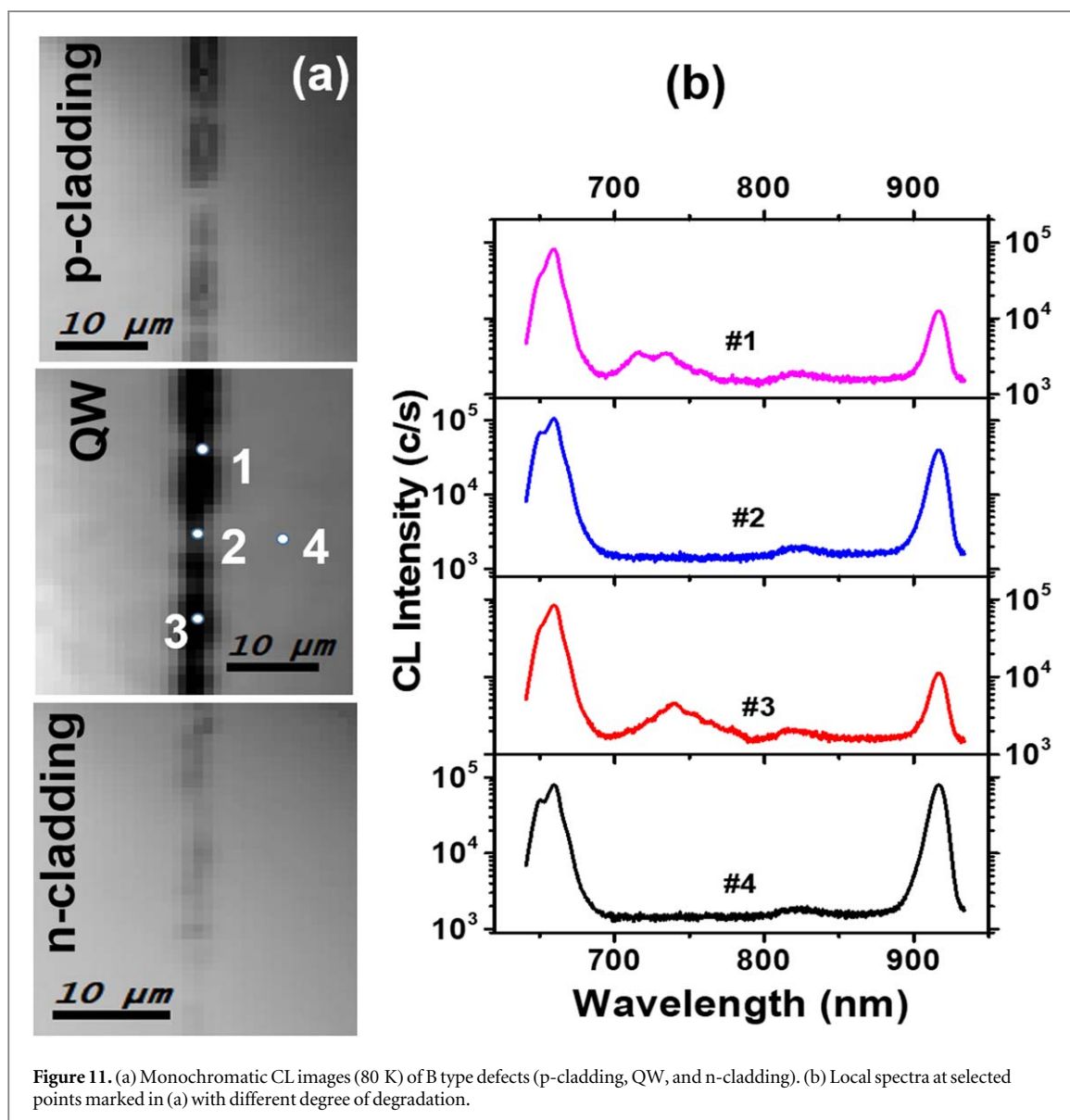


Figure 10. (a) Monochromatic CL images (80 K) of A type defects (p-cladding, QW, and n-cladding). (b) Local spectra (80 K) at selected points marked in (a) with different degree of degradation.

80 K). The emission of the n-type cladding layer is not excited at 10 keV. On the other hand, the transfer of charge to the QW is very low, as deduced from the weak QW emission. Exciting with 15 keV permits to see three emission bands, corresponding to the p-type cladding (649 nm), the QW (916 nm), and the n-type cladding (659 nm). By increasing the e-beam energy to 25 keV, one observes a broadband, convolution of the respective emission bands of the p-type and n-type cladding layers, and the QW emission band. The barrier layers are not observed as the e-h pairs generated on them are transferred to the QW. Also, one starts to see the emission from the GaAs substrate at 820 nm. Once the different CL bands are identified, spectrally resolved CL images (hyperspectral images) will permit to localize the defects of the degraded areas in the laser structure.

Monochromatic images extracted from the hyperspectral images of A type defects are shown in figure 10(a). The emissions of the p-type cladding (649 nm), n-type cladding (659 nm), and QW (916 nm) show that the c-DLDs forming the halo around the ridge only affect the QW emission, which is partially quenched in the halo area, while the cladding layers are free of the influence of these dislocations. One can argue that the arrays of $\langle 100 \rangle$ and $\langle 1-10 \rangle$ oriented dislocations are inhibited to propagate towards the adjacent layers. This might be associated with the endurance of the strained QW, which would behave as a filter for the propagation of these dislocations [89]. The QW emission is fully quenched along the ridge, while the emission of the p-type cladding is enhanced, and the emission from the n-type cladding layer is partially quenched. Some representative local spectra are plotted in figure 10(b) corresponding to the points marked in the CL image. The CL emission enhancement in the p-cladding layer might be related to the formation of a potential barrier at the interface with the p-type barrier layer, which inhibits the transfer of the free carriers towards the QW. This potential barrier can be created by the segregation of Al towards the interface cladding/barrier, forming an Al-rich AlGaAs alloy, as it was shown to occur in [77].

The hyperspectral images of B type defects reveal a different behavior with respect to A type defects, figure 11(a). The three monochromatic images, corresponding to p-type cladding, QW, and n-type cladding layers, present similar patterns. The QW emission is irregularly quenched along the ridge, with discontinuities showing up in the dark pattern. The regions with the highest quenching level spread out of the ridge limits; these zones are those that appear also quenched in the monochromatic images of the two cladding layers. Selected spectra of zones with different degree of degradation are plotted in figure 11(b). Another point to consider is the fact that, unlike the A type defects, the QW is not fully quenched in B type defects. The QW emission profiles along the ridge for the two defect types are displayed in figure 12: while full quenching of the QW emission is



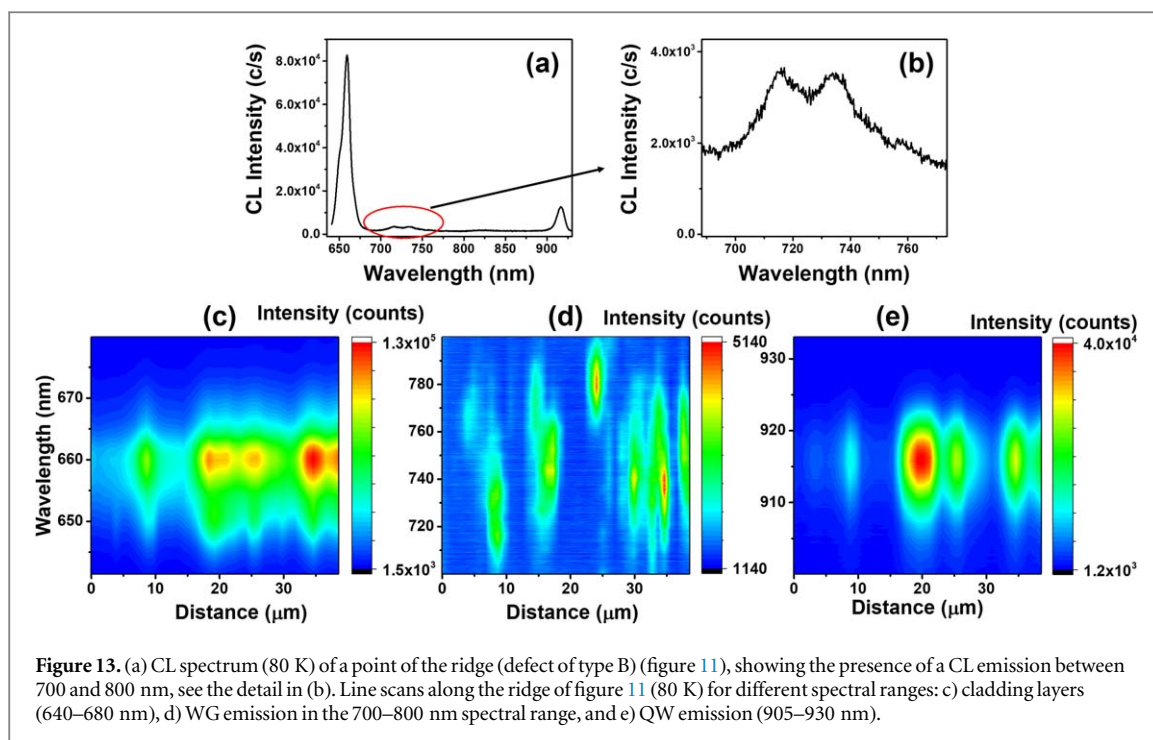


Figure 13. (a) CL spectrum (80 K) of a point of the ridge (defect of type B) (figure 11), showing the presence of a CL emission between 700 and 800 nm, see the detail in (b). Line scans along the ridge of figure 11 (80 K) for different spectral ranges: c) cladding layers (640–680 nm), d) WG emission in the 700–800 nm spectral range, and e) QW emission (905–930 nm).

observed for the A type defects, the QW is still emitting, even if substantially reduced, all along the ridge for B type defects.

A spectrum of the B type defects is shown in figure 13(a). One observes an additional emission between 700 and 800 nm in the damaged regions. Interestingly, this emission appears very irregular both in intensity and in its spectral shape depending on the position along the ridge. This emission seems to be related to the barrier layers, both p and n: we label it as the waveguide band (WG).

A CL line scan along the ridge of the laser section shown in figure 11 is plotted in figure 13. The spectral fluctuations of the WG band are clearly appreciated, while the bands associated with the QW and the claddings do not show spectral changes other than the intensity. The fluctuations in the spectral emission distribution between 700 and 800 nm suggest changes in the composition of the barrier layers. It points to the formation of domains of different composition, consequence of the degradation. These emission bands appear irregularly distributed along the DLD, figure 13(d).

7. Summary

We have presented an overview of the application of CL to the study of the laser diode degradation, which is extensible to other devices. The lateral and in-depth resolution of the CL make it suitable for studying the defects issued from the laser degradation. Combined with its spectroscopic capabilities, this renders CL as an ideal tool to study multilayer structures, such as laser diodes. The observation of the defects resulting from the degradation of laser diodes has allowed us to set up a model for describing the COD. This model is based on the thermal stress induced by the local heating produced by non-radiative recombination and subsequent laser radiation self absorption at tiny regions (microscopic or submicroscopic) of the active zone of the laser [36, 69, 71, 90–92]. The local heating can occur at both the front mirror and/or inside the cavity. The local temperature increase induces a local shrinkage in the bandgap, so that laser self-absorption becomes relevant in these limited volumes and launches the COD process.

Spectrally resolved CL has been scarcely used to study the degradation of lasers, which were mainly studied through EBIC and pan-CL images, which reveal the defect morphology but do not provide the information linking the defects to the different layers of the active zone of the laser. In this sense, hyperspectral images provide capital information about the damage localization in the laser structure, in particular, about what layers of the laser structure are concerned by the degradation. By controlling the different parameters of the CL in the SEM one can build up a post-mortem degradation scenario.

The discontinuous dark contrast along the DLDs, revealing different states of degradation along the lines, rules out the propagation of a molten front as the cause of the DLD formation. A scenario in which one

combines the sensitization of the cavity by the formation of point defects, combined with self-focusing caused by the hot spots (thermal lensing), can account for the conditions necessary for the formation of the DLDs resulting from the degradation [93]. The spectroscopic analysis of the damaged regions shows that the damage extends to the barrier layers, also, the cladding layers can be affected. This implies that not only the gain is reduced by degradation (QW degradation), but also the resonant cavity is seriously damaged leading to the abrupt end of lasing.

Acknowledgments

This work was funded by Junta de Castilla y Leon and FEDER (contract VA283P18) and Spanish Ministry of Competitiveness (contract ENE- 2017-89561-C4-3-R).

Data availability statement

All data that support the findings of this study are included within the article (and any supplementary files).

ORCID iDs

S Dadgostar  <https://orcid.org/0000-0003-3708-0561>

J Souto  <https://orcid.org/0000-0002-3676-1712>

J Jiménez  <https://orcid.org/0000-0001-6079-332X>

References

- [1] Gilliland G D 1997 Photoluminescence spectroscopy of crystalline semiconductors *Mater. Sci. Eng. R Reports* **18** 99–399
- [2] Pavesi L and Guzzi M 1994 Photoluminescence of Al_xGa_{1-x}As alloys *J. Appl. Phys.* **75** 4779–842
- [3] Reshchikov M A and Morkoç H 2005 Luminescence properties of defects in GaN *J. Appl. Phys.* **97** 061301
- [4] Baeumler M and Jantz W 2003 *Microprobe Characterization of Optoelectronic Materials* ed J Jimenez (New York: Taylor and Francis)
- [5] Martin E, Landesman J P, Hirtz J P and Fily A 1999 Microphotoluminescence mapping of packaging-induced stress distribution in high-power AlGaAs laser diodes *Appl. Phys. Lett.* **75** 2521–3
- [6] Holst J, Kaschner A, Hoffmann A, Fischer P, Bertram F, Riemann T, Christen J, Hiramatsu K, Shibata T and Sawaki N 1999 Time-resolved microphotoluminescence of epitaxial laterally overgrown GaN *Appl. Phys. Lett.* **75** 3647–9
- [7] Mahadik N A et al 2011 Structure and morphology of inclusions in 4° offcut 4H-SiC epitaxial layers *J. Electron. Mater.* **40** 413–8
- [8] Okamoto K, Tateishi K, Tamada K, Funato M and Kawakami Y 2019 Micro-photoluminescence mapping of surface plasmon-coupled emission from InGa_N/Ga_N quantum wells *Jpn. J. Appl. Phys.* **58** SCCB31
- [9] Braithwaite J, Silver M, Wilkinson V A, O'Reilly E P and Adams A R 1995 Role of radiative and nonradiative processes on the temperature sensitivity of strained and unstrained 1.5 μm InGaAs(P) quantum well lasers *Appl. Phys. Lett.* **67** 3546–8
- [10] Polyakov A Y, Smirnov N B, Govorkov A V, Amano H, Pearton S J, Lee I-H, Sun Q, Han J and Karpov S Y 2011 Role of nonradiative recombination centers and extended defects in nonpolar GaN on light emission efficiency *Appl. Phys. Lett.* **98** 072104
- [11] Gustafson A and Samuelson L 2003 *Microprobe Characterization of Optoelectronic Materials* ed J Jimenez (New York: Taylor and Francis)
- [12] Yacobi B G and Holt D B 1986 Cathodoluminescence scanning electron microscopy of semiconductors *J. Appl. Phys.* **59** R1–24
- [13] Brillson L J 2012 Applications of depth-resolved cathodoluminescence spectroscopy *J. Phys. D: Appl. Phys.* **45** 183001
- [14] Dierre B, Yuan X L, Ohashi N and Sekiguchi T 2008 Effects of specimen preparation on the cathodoluminescence properties of ZnO nanoparticles *J. Appl. Phys.* **103** 083551
- [15] Jimenez J and Tomm J W 2016 Photoluminescence (PL) techniques *Springer Series in Optical Sciences* (Berlin: Springer)
- [16] Herman M A, Bimberg D and Christen J 1991 Heterointerfaces in quantum wells and epitaxial growth processes: evaluation by luminescence techniques *J. Appl. Phys.* **70** R1–52
- [17] Fukuda M 1991 *Reliability and Degradation of Semiconductor Lasers and LEDs* (Boston. London: Artech House Publisher)
- [18] Ueda O 1996 *Reliability Degradation of III-V Optical Devices, LEDs* (London: Artech House Publishers)
- [19] Hakki B W and Paoli T L 1973 cw degradation at 300 °K of GaAs double-heterostructure junction lasers. II. Electronic gain *J. Appl. Phys.* **44** 4113–9
- [20] Wallace M J, Edwards P R, Kappers M J, Hopkins M A, Oehler F, Sivaraya S, Allsopp D W E, Oliver R A, Humphreys C J and Martin R W 2014 Bias dependence and correlation of the cathodoluminescence and electron beam induced current from an InGa_N/Ga_N light emitting diode *J. Appl. Phys.* **116** 033105
- [21] Wen P, Zhang S, Liu J, Li D, Zhang L, Zhou K, Su X, Tian A, Zhang F and Yang H 2016 Catastrophic degradation of InGa_N/Ga_N blue laser diodes *IEEE Trans. Device Mater. Reliab.* **16** 638–41
- [22] Besendörfer S, Meissner E, Tajalli A, Meneghini M, Freitas J A, Derluyn J, Medjdoub F, Meneghesso G, Friedrich J and Erlbacher T 2020 Vertical breakdown of GaN on Si due to V-pits *J. Appl. Phys.* **127** 015701
- [23] Lin C-H, Merz T A, Doutt D R, Hetzer M J, Joh J, del Alamo J A, Mishra U K and Brillson L J 2009 Nanoscale mapping of temperature and defect evolution inside operating AlGa_N/Ga_N high electron mobility transistors *Appl. Phys. Lett.* **95** 033510
- [24] Pomeroy J W, Kuball M, Uren M J, Hilton K P, Balmer R S and Martin T 2006 Insights into electroluminescent emission from AlGa_N/Ga_N field effect transistors using micro-Raman thermal analysis *Appl. Phys. Lett.* **88** 1–3
- [25] Souto J, Pura J L and Jiménez J 2016 About the physical meaning of the critical temperature for catastrophic optical damage in high power quantum well laser diodes *Laser Phys. Lett.* **13** 025005

- [26] Young A P and Brillson L J 2000 Luminescence spectroscopy of GaN in the high-temperature regime from room temperature to 900 °C *Appl. Phys. Lett.* **77** 699–701
- [27] Kimerling L C 1978 Recombination enhanced defect reactions *Solid. State. Electron.* **21** 1391–401
- [28] Nakwaski W 1985 Thermal analysis of the catastrophic mirror damage in laser diodes *J. Appl. Phys.* **57** 2424–30
- [29] Moser A, Latta E E and Webb D J 1989 Thermodynamics approach to catastrophic optical mirror damage of AlGaAs single quantum well lasers *Appl. Phys. Lett.* **55** 1152–4
- [30] Eliseev P G 1996 Optical strength of semiconductor laser materials *Prog. Quantum Electron.* **20** 1–82
- [31] Hempel M, Tomm J W, Ziegler M, Elsaesser T, Michel N and Krakowski M 2010 Catastrophic optical damage at front and rear facets of diode lasers *Appl. Phys. Lett.* **97** 231101
- [32] Ziegler M, Hempel M, Larsen H E, Tomm J W, Andersen P E, Clausen S, Elliott S N and Elsaesser T 2010 Physical limits of semiconductor laser operation: a time-resolved analysis of catastrophic optical damage *Appl. Phys. Lett.* **97** 021110
- [33] Sin Y, Lingley Z, Presser N, Brodie M, Ives N and Moss S C 2017 Catastrophic optical bulk damage in high-power InGaAs-AlGaAs strained quantum well lasers *IEEE J. Sel. Top. Quantum Electron.* **23** 1–13
- [34] Moser A and Latta E E 1992 Arrhenius parameters for the rate process leading to catastrophic damage of AlGaAs-GaAs laser facets *J. Appl. Phys.* **71** 4848–53
- [35] Sin Y, Presser N, Brodie M, Lingley Z, Foran B and Moss S C 2015 Degradation mechanisms in high-power multi-mode InGaAs-AlGaAs strained quantum well lasers for high-reliability applications *High-Power Diode Laser Technology and Applications XIII* ed M S Zediker (Bellingham: SPIE) p 93480L (<https://doi.org/10.1117/12.2076788>)
- [36] Martín-Martín A, Avella M, Iñiguez M P, Jiménez J, Oudart M and Nagle J 2009 Thermomechanical model for the plastic deformation in high power laser diodes during operation *J. Appl. Phys.* **106** 073105
- [37] Salvati G, Lazzarini L, Sekiguch T and Chen B 2011 Assessment of semiconductors by scanning electron microscopy techniques *Comprehensive Semicond. Sci. Technol.* **4** 308–56
- [38] Petroff P and Hartman R L 1974 Rapid degradation phenomenon in heterojunction GaAlAs-GaAs lasers *J. Appl. Phys.* **45** 3899–903
- [39] Henry C H, Petroff P M, Logan R A and Merritt F R 1979 Catastrophic damage of Al_xGa_{1-x}As double-heterostructure laser material *J. Appl. Phys.* **50** 3721–32
- [40] Mahajan S, Temkin H and Logan R A 1984 Formation of optically induced catastrophic degradation lines in InGaAsP epilayers *Appl. Phys. Lett.* **44** 119–21
- [41] Jakubowicz A 1997 Material and fabrication-related limitations to high-power operation of GaAs/AlGaAs and InGaAs/AlGaAs laser diodes *Mater. Sci. Eng. B* **44** 359–63
- [42] Häusler K, Zeimer U, Sumpf B, Erbert G and Tränkle G 2008 Degradation model analysis of laser diodes *J. Mater. Sci., Mater. Electron.* **19** 160–4
- [43] Pommès M, Avella M, Cánovas E, Jiménez J, Fillardet T, Oudart M and Nagle J 2005 Cation intermixing at quantum well/barriers interfaces in aged AlGaAs-based high-power laser diodes bars *Appl. Phys. Lett.* **86** 131103
- [44] Hortelano V, Anaya J, Souto J, Jiménez J, Perinet J and Laruelle F 2013 Defect signatures in degraded high power laser diodes *Microelectron. Reliab.* **53** 1501–5
- [45] Meneghini M et al 2013 Degradation of InGaN/GaN laser diodes investigated by micro-cathodoluminescence and micro-photoluminescence *Appl. Phys. Lett.* **103** 233506
- [46] Gachet D, de Santi C, Meneghini M, Mura G, Vanzi M, Meneghesso G and Zanoni E 2016 High-resolution cathodoluminescence investigation of degradation processes in InGaN green laser diodes *Microsc. Microanal.* **22** 1738–9
- [47] Tomm J W and Jiménez J 2007 *Quantum-Well Laser Array Packaging* (New York: McGraw-Hill)
- [48] Hosokawa T, Fujimura S, Yabuuchi Y, Tsukamoto Y, Porporati A A, Zhu W and Pezzotti G 2011 Nanometer-scale cathodoluminescence analysis of GaAs and its application to the assessment of laser diode *Phys. Status Solidi Appl. Mater. Sci.* **208** 1000–11
- [49] Everhart T E and Hoff P H 1971 Determination of kilovolt electron energy dissipation vs penetration distance in solid materials *J. Appl. Phys.* **42** 5837–46
- [50] Bonard J, Ganière J, Akamatsu B, Araújo D and Reinhart F 1996 Cathodoluminescence study of the spatial distribution of electron-hole pairs generated by an electron beam in Al_{0.4}Ga_{0.6}As *J. Appl. Phys.* **79** 8693–703
- [51] Drouin D, Coutre A R, Gauvin R, Hovington P, Horny P and Demers H 2006 Monte Carlo Simulation of Electron Trajectories in Solids (CASINO) Canada University of Sherbrooke, Quebec
- [52] Araújo D, Oelgart G, Ganière J D and Reinhart F K 1994 Comparison of the lateral carrier transport between a GaAs single quantum well and the AlGaAs barrier during cathodoluminescence excitation *J. Appl. Phys.* **76** 342–6
- [53] Barjon J, Brault J, Daudin B, Jalabert D and Sieber B 2003 Cathodoluminescence study of carrier diffusion in AlGaIn *J. Appl. Phys.* **94** 2755–7
- [54] Niemeyer M, Ohlmann J, Walker A W, Kleinschmidt P, Lang R, Hannappel T, Dimroth F and Lackner D 2017 Minority carrier diffusion length, lifetime and mobility in p-type GaAs and GaInAs *J. Appl. Phys.* **122** 115702
- [55] Dadgostar S, Belloso Casuso C, Martínez O, Hinojosa M, García I and Jiménez J 2020 A Cathodoluminescence study on the diffusion length in AlGaInP/InGaP/AlInP solar cell heterostructures *J. Electron. Mater.* **49** 5184–9
- [56] Donolato C 1979 Contrast and resolution of SEM charge-collection images of dislocations *Appl. Phys. Lett.* **34** 80–1
- [57] Bruckbauer J, Edwards P R, Wang T and Martin R W 2011 High resolution cathodoluminescence hyperspectral imaging of surface features in InGaIn/GaN multiple quantum well structures *Appl. Phys. Lett.* **98** 141908
- [58] Massabuau F C P et al 2017 Carrier localization in the vicinity of dislocations in InGaIn *J. Appl. Phys.* **121** 013104
- [59] Brassier C, Bruckbauer J, Gong Y, Jiu L, Bai J, Warzecha M, Edwards P R, Wang T and Martin R W 2018 Cathodoluminescence studies of chevron features in semi-polar (112̄2) InGaIn/GaN multiple quantum well structures *J. Appl. Phys.* **123** 174502
- [60] Edwards P R and Martin R W 2011 Cathodoluminescence nano-characterization of semiconductors *Semicond. Sci. Technol.* **26** 064005
- [61] Liu W, Carlin J-F, Grandjean N, Deveaud B and Jacopin G 2016 Exciton dynamics at a single dislocation in GaN probed by picosecond time-resolved cathodoluminescence *Appl. Phys. Lett.* **109** 042101
- [62] Hortelano V, Martínez O, Cuscó R, Artús L and Jiménez J 2016 Cathodoluminescence study of Mg activation in non-polar and semi-polar faces of undoped/Mg-doped GaN core-shell nanorods *Nanotechnology* **27** 095706
- [63] Waters R G 1991 Diode laser degradation mechanisms: a review *Prog. Quantum Electron.* **15** 153–74
- [64] Jiménez J 2003 Laser diode reliability: crystal defects and degradation modes *Comptes Rendus Phys.* **4** 663–73
- [65] Epperlein P W 2013 *Semiconductor Laser Engineering, Reliability and Diagnostics* (New York: Wiley)
- [66] Bettinati M A 2013 High optical strength GaAs-based laser structures *Microelectron. Reliab.* **53** 1496–500

- [67] Sin Y, Lingley Z, Ayvazian T, Brodie M and Ives N 2018 Catastrophic optical bulk damage—a new failure mode in high-power InGaAs-AlGaAs strained quantum well lasers *MRS Adv.* **3** 3329–45
- [68] Chen G and Tien C L 1993 Facet heating of quantum well lasers *J. Appl. Phys.* **74** 2167–74
- [69] Souto J, Pura J L and Jiménez J 2019 Thermomechanical issues of high power laser diode catastrophic optical damage *J. Phys. D: Appl. Phys.* **52** 343002
- [70] Tomm J W, Ziegler M, Hempel M and Elsaesser T 2011 Mechanisms and fast kinetics of the catastrophic optical damage (COD) in GaAs-based diode lasers *Laser Photon. Rev.* **5** 422–41
- [71] Souto J, Pura J L and Jiménez J 2017 Nanoscale effects on the thermal and mechanical properties of AlGaAs/GaAs quantum well laser diodes: influence on the catastrophic optical damage *J. Phys. D: Appl. Phys.* **50** 235101
- [72] Hempel M, Tomm J W, Venables D, Rossin V, Zucker E and Elsaesser T 2015 Long-term aging and quick stress testing of 980 nm single-spatial mode lasers *J. Light. Technol.* **33** 4450–6
- [73] Martín-Martín A, Avella M, Pommiès M, Jiménez J, Iñiguez M P, Oudart M and Nagle J 2008 Study of the degradation of AlGaAs-based high-power laser bars: v defects *J. Mater. Sci., Mater. Electron.* **19** 140–4
- [74] Andrianov A V, Dods S R A, Morgan J, Orton J W, Benson T M, Harrison I, Larkins E C, Daiminger F X, Vassilakis E and Hirtz J P 2000 Optical and photoelectric study of mirror facets in degraded high power AlGaAs 808 nm laser diodes *J. Appl. Phys.* **87** 3227–33
- [75] Tomm J W, Gerhardt A, Müller R, Malyarchuk V, Sainte-Marie Y, Galtier P, Nagle J and Landesman J P 2003 Spatially resolved spectroscopic strain measurements on high-power laser diode bars *J. Appl. Phys.* **93** 1354–62
- [76] Hempel M, Tomm J W, Bachmann A, Lauer C, Furlitsch M, Strauß U and Elsaesser T 2016 Transient surface modifications during singular heating events at diode laser facets *Semicond. Sci. Technol.* **31** 055007
- [77] Hempel M, Tomm J W, La Mattina F, Ratschinski I, Schade M, Shorubalko I, Stiefel M, Leipner H S, Kießling F M and Elsaesser T 2013 Microscopic origins of catastrophic optical damage in diode lasers *IEEE J. Sel. Top. Quantum Electron.* **19** 1500508 (1–8)
- [78] Hempel M, Tomm J W, Elsaesser T and Bettiati M 2012 High single-spatial-mode pulsed power from 980 nm emitting diode lasers *Appl. Phys. Lett.* **101** 191105
- [79] Oh-hori T, Itoh H, Tanaka H, Kasai K, Takikawa M and Komeno J 1987 Donor-cation vacancy complex in Si-doped AlGaAs grown by metalorganic chemical vapor deposition *J. Appl. Phys.* **61** 4603–5
- [80] Pavesi L, Ky N H, Ganière J D, Reinhart F K, Baba-Ali N, Harrison I, Tuck B and Henini M 1992 Role of point defects in the silicon diffusion in GaAs and Al_{0.3}Ga_{0.7}As and in the related superlattice disordering *J. Appl. Phys.* **71** 2225–37
- [81] Hempel M, La Mattina F, Tomm J W, Zeimer U, Broennimann R and Elsaesser T 2011 Defect evolution during catastrophic optical damage of diode lasers *Semicond. Sci. Technol.* **26** 075020
- [82] Hempel M, Tomm J W, Hortelano V, Michel N, Jimenez J, Krakowski M and Elsaesser T 2012 Time-resolved reconstruction of defect creation sequences in diode lasers *Laser Photon. Rev.* **6** L15–9
- [83] Waters R G, Bour D P, Yellen S L and Ruggieri N F 1990 Inhibited dark-line defect formation in strained InGaAs/AlGaAs quantum well lasers *IEEE Photonics Technol. Lett.* **2** 531–3
- [84] Wunsch D C and Bell R R 1968 Determination of threshold failure levels of semiconductor diodes and transistors due to pulse voltages *IEEE Trans. Nucl. Sci.* **15** 244–59
- [85] Petroff P M and Kimerling L C 1976 Dislocation climb model in compound semiconductors with zinc blende structure *Appl. Phys. Lett.* **29** 461–3
- [86] Kamejima T and K Ishida J M 1977 Related content injection-enhanced dislocation glide under uniaxial stress in GaAs-(GaAl) as double heterostructure laser *Jpn. J. Appl. Phys.* **16** 233–40
- [87] O'Hara S, Hutchinson P W and Dobson P S 1977 The origin of dislocation climb during laser operation *Appl. Phys. Lett.* **30** 368–71
- [88] Maeda K, Sato M, Kubo A and Takeuchi S 1983 Quantitative measurements of recombination enhanced dislocation glide in gallium arsenide *J. Appl. Phys.* **54** 161–8
- [89] Hoagland R G, Kurtz R J and Henager C H 2004 Slip resistance of interfaces and the strength of metallic multilayer composites *Scr. Mater.* **50** 775–9
- [90] Martín-Martín A, Avella M, Iñiguez M P, Jiménez J, Oudart M and Nagle J 2008 A physical model for the rapid degradation of semiconductor laser diodes *Appl. Phys. Lett.* **93** 171106
- [91] Martín-Martín A, Iñiguez P, Jiménez J, Oudart M and Nagle J 2011 Role of the thermal boundary resistance of the quantum well interfaces on the degradation of high power laser diodes *J. Appl. Phys.* **110** 033113
- [92] Souto J, Pura J L and Jiménez J 2018 Thermal and mechanical issues of high-power laser diode degradation *MRS Commun.* **8** 995–9
- [93] Pura J L, Souto J and Jiménez J 2020 Effect of thermal lensing and the micrometric degraded regions on the catastrophic optical damage process of high-power laser diodes *Opt. Lett.* **45** 1667